ACS APPLIED MATERIALS & INTERFACES

Research Article

Cite This: ACS Appl. Mater. Interfaces 2019, 11, 13927−13934

www.acsami.org

In Operando Observation of Neuropeptide Capture and Release on Graphene Field-Effect Transistor Biosensors with Picomolar Sensitivity

Steve Kim,[†,#] Li Xing,[‡,∥,#] Ahmad E. Islam,[‡,∥] Ming-Siao Hsiao,[‡,∥,¶] Yen Ngo,[†,∥] Oksana M. Pavlyuk,[§] Rhett L. Martineau,[‡,∥] Cheri M. Hampton,[‡,∥] Cameron Crasto,[‡,∥] Joseph Slocik,[‡,∥] Madhavi P. Kadakia,[§] Joshua A. Hagen,[⊥] Nancy Kelley-Loughnane,[‡] Rajesh R. Naik,[†] and Lawrence F. Drummy*[,‡]

[†]711th Human Performance Wing, and [‡]Materials and Manufacturing Directorate, Air Force Research Laboratory, Wright Patterson AFB, Ohio 45433, United States

[§]Department of Biochemistry and Molecular Biology, Wright State University, Dayton, Ohio 45431, United States

[∥]Biological and Nanoscale Technologies Division, UES Inc., Dayton, Ohio 45432, United States

[⊥]Rockefeller Neuroscience Institute, School of Medicine, West Virginia University, Morgantown, West Virginia 26506, United States

Supporting Information

ABSTRACT: Transmission electron microscopy (TEM) is being pushed to new capabilities which enable studies on systems that were previously out of reach. Among recent innovations, TEM through liquid cells (LC-TEM) enables *in operando* observation of biological phenomena. This work applies LC-TEM to the study of biological components as they interact on an abiotic surface. Specifically, analytes or target molecules like neuropeptide Y (NPY) are observed *in operando* on functional graphene field-effect transistor (GFET) biosensors. Biological recognition elements (BREs) identified using biopanning with affinity to NPY are used to functionalize graphene to obtain selectivity. On working devices capable of achieving picomolar responsivity to neuropeptide Y, LC-TEM reveals translational motion, stochastic positional fluctuations due to constrained Brownian motion, and rotational dynamics of captured analyte. Coupling these observations with the electrical responses of the GFET biosensors in response to analyte capture and/or release will potentially enable new insights leading to more advanced and capable biosensor designs.

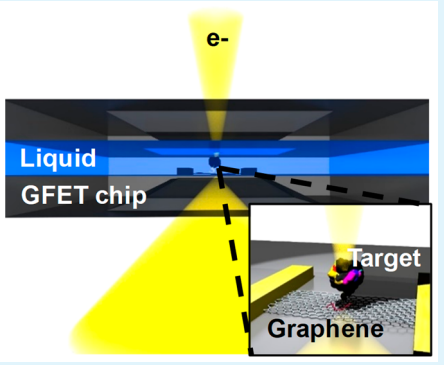

KEYWORDS: *In operando, neuropeptide-Y, liquid-cell, transmission electron microscopy, cryo-electron microscopy, graphene, peptides, sensitivity, selectivity.*

INTRODUCTION

Biosensors based on biofunctionalized graphene field-effect transistors (GFETs) present opportunities for label-free sensors with extreme sensitivity.[1−6] Because of their high sensitivity, GFETs are poised to enable new applications including the tracking of low-abundance hormones and neurotransmitters in sweat or tears. However, a number of obstacles impede progress toward reliable devices and significant research and development is required to deliver real-world devices. To date, the physics surrounding signal generation by analytes captured near graphene surfaces remains imperfectly understood and thus tools to study analyte interactions with sensor surfaces over the course of signal transduction events are valuable for advancing biosensor development efforts.

Recently, inroads have been made into studying biological molecules in their native environment with electron microscopy at high resolution. TEM imaging through thin sections of liquids, known as liquid-cell transmission electron microscopy (LC-TEM), has been demonstrated on a number of biological samples including whole cells,[7] liposomes,[8] and viruses.[9] LC-TEM enables ultrahigh resolution imaging of biological components in an environment which more ideally matches the native environment[10] enabling *in operando*, direct visualization of sensor activity.

Peptides with binding affinity to a number of molecular targets have been developed by many research laboratories using phage display.[11−20] The motivations behind using short peptide fragments as biological recognition elements (BREs) include a theoretically high sensitivity to analyte capture given their short length and proximity to a sensor surface, ease of manufacture and modification, and an increased shelf life in comparison with many other BREs including antibodies. Peptide BREs can be designed with two domains to enable

Received: November 21, 2018
Accepted: March 18, 2019
Published: March 18, 2019

DOI: 10.1021/acsami.8b20498
ACS Appl. Mater. Interfaces 2019, 11, 13927−13934

functionalization onto a sensor surface by a first domain and capture of an analyte of interest by a second domain. In this work, we develop GFET biosensors based on phage display peptides and characterize their performance using the electrical performance of the GFET biosensors and also via direct visualization of BRE/analyte activity on the GFET surfaces using LC-TEM.

We have chosen to study peptide BRE capture of the neurotransmitter neuropeptide Y (NPY) onto GFET surfaces. NPY is one of the most important neuropeptides found within both the central and peripheral nervous systems of the human body[21−23] and is involved in regulation of biological and pathophysiological functions such as food uptake, energy homeostasis, circadian rhythm, and cognition. In vivo, NPY is translated from mRNA as prepro-peptide of 97 amino acids. After cleavage of the signal peptide, proteolytic processing, and amidation, a 36 amino acid peptide is released and circulated as mature signal peptide with the sequence YPSKPDNPGEDAPAEDMARYYSALRHYINLITRQRY.

Although NPY is principally found in the tissues and fluids of the nervous system and in blood, a small fraction partitions into sweat and is thus available for noninvasive assessment. In healthy individuals, NPY presents in sweat in the range of 0.8−2.9 pM. In individuals with major depressive disorder, the levels rise to 14.2−73.2 pM.[24] In the picomolar concentration range, NPY is a challenging analyte tractable by only the most sensitive modalities yet is within the reported detection limits of graphene field-effect transistors (GFETs).[25,26]

We hypothesized that it might be possible to use LC-TEM to make molecular level, time-resolved observations that could be used to understand and optimize sensor performance. Ideally one would correlate the electrical activity of NPY binding to GFET biosensors while simultaneously observing component interactions and dynamics using LC-TEM with the expectation that direct observations would provide insights to guide sensor design. Figure 1 shows a general schematic of an experimental setup enabling electrical measurements of GFET response with concurrent direct visualization via LC-TEM. This setup, and subsets thereof, were used to study NPY capture onto graphene surfaces.

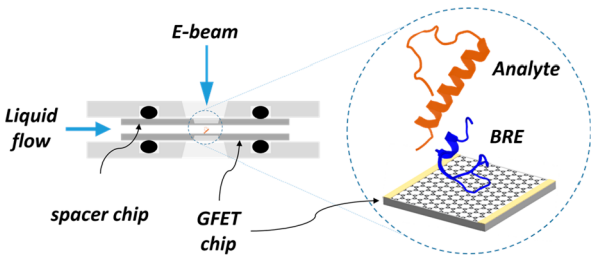

Figure 1. LC-TEM imaging of peptide-functionalized GFETs. *In operando* studies of analyte capture by peptide-based biological recognition elements (BREs) is made possible by TEM-compatible GFETs housed within a TEM-holder with fluidic and electrical interconnects. TEM-compatible chips containing graphene (GFET chip) are made by spanning monolayer graphene between the electrodes on the chip. BREs functionalized on graphene of such chips allow selective capture of a specific analyte that can be detected by monitoring changes in the conductivity of graphene. The liquid-cell (LC) is formed by placing a spacer chip with a spacer thickness ∼100 nm on top of the functionalized GFET chip that creates a fluid path along the surface of graphene enabling the *in operando* sensor study. O-rings shown in the cross-section provide a fluid-tight seal.

RESULTS AND DISCUSSION

Biopanning for Identification of Peptides. We have previously identified and characterized a 12-mer peptide with high selectivity, binding affinity, and specificity for graphene using a peptide phage library.[12−16,27,28] The peptide, named P1, consists of the sequence HSSYWYAFNNKT.[29] Biopanning was also used to discover peptides with affinity to NPY. Details can be found in the Supporting Information, Section S1.1. Through an affinity selection process known as biopanning, phages displaying peptides with high affinity for the target molecule are isolated, eluted, and amplified. At the onset of our study, streptavidin (SA)-coated magnetic beads were functionalized with biotinylated NPY (bNPY) and used as target for peptide phage display studies. Four rounds of biopanning were performed using bNPY with a Ph.D.-12 library (New England Biolabs, Inc., Ipswich, MA) and several dominant sequences were enriched. We focused on the three distinct peptides labeled N1, N2, and N3 exhibiting basic isoelectric point (pI) of around 8.5−9.9, as shown in Figure 2B. The equilibrium constant (K_{eq}) values for these peptides

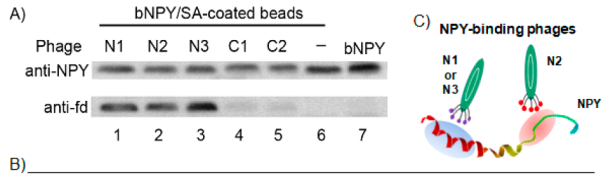

B)

Peptide	Sequence	Calculated pI	K_{eq} (M^{-1})
N1	VQHNTKYSVVIR	9.99	3.30 x 10^4
N2	YHPNGMNPYTKA	8.50	1.03 x 10^5
N3	FPNWSLRPMNQM	9.75	4.18 x 10^4

Figure 2. Binding confirmation of phages displaying NPY binding peptides. (A) Equivalent amounts of phage displaying NPY (lanes 1−3) or SA binding peptides (lanes 4−5) were incubated with biotinylated NPY (bNPY) immobilized on SA-coated magnetic beads. Lane 6 represents bNPY immobilized on SA-coated magnetic beads and lane 7 represents bNPY peptide as controls. (B) The amino acid sequences, isoelectric points (pI), and equilibrium constants (K_{eq}, for a Langmuir adsorption isotherm obtained from QCM measurements) of NPY-binding peptides are tabulated. (C) Schematic representation of binding sites of BREs on NPY, as per CD spectra. N2 binds to the unstructured region of NPY, whereas N1 and N3 bind to the helical region.

were also calculated by fitting the response to multiple concentrations of NPY (measured using quartz crystal microbalance, QCM) using Langmuir adsorption isotherm (see Supporting Information, Figure S2C). All three peptides were found to contain hydrophobic and aromatic amino acids which are known to be involved in protein−protein interactions.[30] As a control, when SA-coated magnetic beads were used as a target in phage display studies, peptide sequences C1 and C2 were isolated which contained the HPQ motif characteristic of streptavidin binding peptides (Supporting Information, Figure S1B).[31]

To confirm the binding interactions of isolated phage clones (N1, N2, and N3) to NPY, we incubated equivalent amounts of the amplified phages displaying either the NPY-binding peptides or control peptides against bNPY-SA magnetic beads or SA beads alone. The phage-bead complexes were rinsed several times with buffer to remove unbound phages and resolved using SDS-PAGE. Immunoblotting with NPY (anti-NPY) or M13 phage coat specific (anti-fd) antibodies was then performed to detect for the presence of NPY on the beads and

DOI: 10.1021/acsami.8b20498
ACS Appl. Mater. Interfaces 2019, 11, 13927−13934

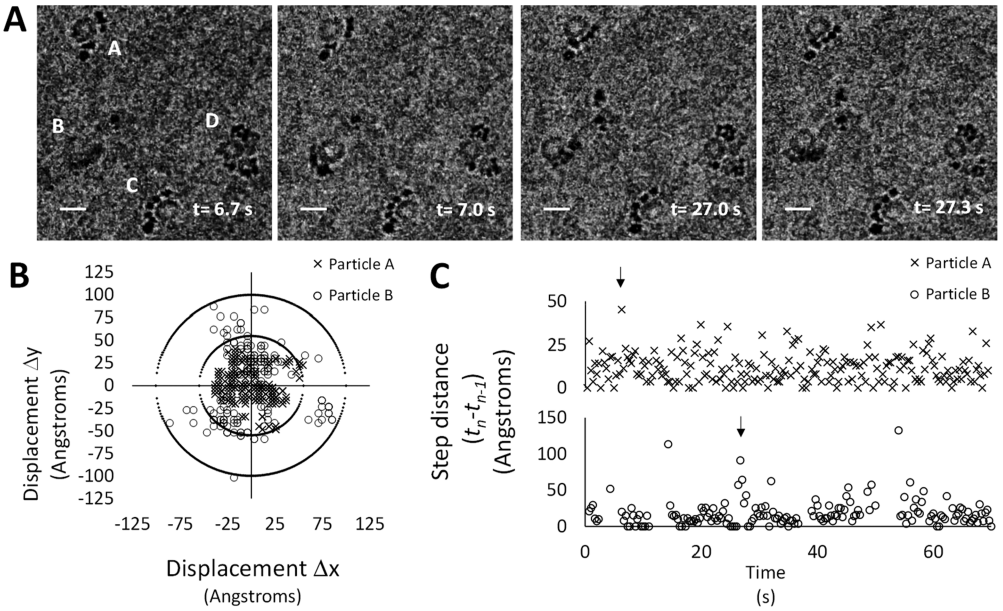

Figure 3. Analysis of motion in BRE-tethered NPY assemblies. Panel A presents LC-TEM micrographs of four NPY assemblies (labeled A−D) tethered to a graphene surface via PBASE and P1N3, taken from a 74 s video. Two of the assemblies (A+B) exhibit significant motion during video capture, whereas assemblies C and D are comparatively static. Assembly A shows significant rotational motion as evidenced in frames captured at 6.7 and 7.0 s. Assembly B shows both rotational and translational motion, with both a large step displacement and rotation on exhibit between frames captured at 27.0 and 27.3 s. Panel B shows the Δx and Δy displacements for assemblies A and B, offset and centered by the average displacement of each assembly observed over the course of the video. Circular overlays of roughly 5.5 and 10 nm radius delineate positional envelopes of the assemblies. Panel C shows the displacement between video frames (3 Hz) for assemblies A and B. Step distances at time points corresponding to the LC-TEM images in Panel A are indicated with arrows. Missing data points in the bottom plot in Panel C are the result of assembly B wandering too far out of focus. Scale bar is 20 nm.

phage, respectively. We observed that phage clones representing NPY binding sequences (N1−N3) only bound to bNPY-SA magnetic beads (Figure 2A, lanes 1−3). Phage clones representing peptide binding sequences that bind to streptavidin (C1 and C2) bound to the SA-coated magnetic beads (Figure 2A, lanes 4−5) as shown by immunoblotting with antibody against the phage coat protein. The presence of a band in lanes 1−3 with anti-fd antibodies indicates that isolated phage clones (N1−N3) bound strongly to the immobilized NPY, while the streptavidin binding phages show little or no binding to NPY. We confirmed that NPY was immobilized onto the SA-Dynabeads as indicated by the presence of bands in all lanes when probed with anti-NPY. As expected, strong binding was detected between the streptavidin-coated magnetic beads and the C1 and C2 phages displaying the peptides with HPQ motif. In contrast, NPY binding phage clones (N1, N2, and N3; lanes 1−3) showed negligible binding to streptavidin (Supporting Information, Figure S1A). Therefore, phage clones (N1−N3) specific for binding to NPY were identified from the phage peptide display library.

We next chemically synthesized the N1−N3 peptides and used circular dichroism (CD) spectroscopy to identify the secondary structure of NPY, N1−N3 and their conjugates (Supporting Information, Section S1.3). NPY exhibited an alpha helical secondary structure with characteristic negative peaks at 222 and 208 nm, while the N1−N3 peptides were unstructured with broad negative peaks at 195 nm (see Figure S3), consistent with previous short peptides isolated from phage display.[32] The addition of N3 to NPY resulted in the presence of an isodichroic point and a loss of helicity in the CD spectrum as shown by a decrease in the ratio of ellipticities at 222/208 nm. This suggests that any structural changes observed between NPY and NPY-N3 complexes is due to binding interactions within the helix-forming regions (Figure 2C). In contrast, the CD spectrum of NPY-N2 complexes strongly resembled the CD spectrum of free NPY. Given that N2 has been determined to bind with NPY, this suggests that binding may occur in a location outside of the helix-forming regions of NPY. N1 complexation with NPY results in a CD spectrum with decreased negative ellipticity but with the same peak shape as free NPY and thus N1 is also likely to bind at or near the alpha helical regions.

CD spectrum results were useful in designing a set of NPY-binding peptide domains for simultaneous analyte capture and analyte labeling. Results specifically suggested the possibility of simultaneous binding of NPY with N3 or N1 at the helix-forming amino acids and N2 outside of the helix-forming amino acids (Supporting Information, Section S1.3). Consequently, the capture domain N3 was concatenated to the graphene binding domain P1 using a three-residue glycine linker. The resultant peptide P1N3 is able to bind both graphene and NPY, but it also binds NPY in a manner that simultaneous binding with the alternate NPY binding peptide N2 is also possible. Thus, NPY can be captured near the graphene surface using P1N3, and N2 conjugated with gold nanoparticles can be used to label NPY for enhanced imaging. N2 was therefore conjugated to 10 nm gold nanoparticles (N2−Au) and simultaneous binding of N3 and N2 to NPY was observed using TEM as shown in Supporting Information Figure S4.

Sensor Preparation. A monolayer of graphene was synthesized via chemical vapor deposition,[33,34] transferred to appropriate TEM chips and finally functionalized sequentially

DOI: 10.1021/acsami.8b20498
ACS Appl. Mater. Interfaces 2019, 11, 13927−13934

with P1N3 followed by the analyte. See Supporting Information, Section S2 for details. In some cases, we used 1-pyrenebutyric acid *N*-hydroxysuccinimide ester (PBASE) as a linker between graphene and P1N3. PBASE provides a monolayer coverage on graphene through pi stacking suitable for immobilization of biomolecules[35−37] and also contains a succinimidyl ester that couples to primary amines located at the N-terminus and at Lys11 of P1N3. P1N3 by itself also forms a monolayer without PBASE (see AFM images in Supporting Information, Section S2.4) and hence can act alone for NPY immobilization. The sensor responses to NPY with and without PBASE were also found to be similar.

Dynamics of NPY on Graphene. Dynamics of NPY were best observed in LC-TEM when NPY was in its prepro-peptide form with an N-terminal Glutathione S-transferase (GST) tag (AbCam 112330, Cambridge, USA). Although the ideal sensor will be designed to detect the 36 amino acid NPY peptide, there is precedent for retaining the fusion tag in structural studies. Recently, a 38 kDa maltose binding protein was used to provide structural integrity to a much smaller peptide and to provide mass for aligning and averaging copies of the complex for single particle analysis.[38] We also observe further that GST forms a trimer of dimers (see cryo-TEM of GST-NPY in Supporting Information, Section S3.1). The resulting hexamer assembly has a diameter of ∼20 nm, which is discernible even through water using TEM. Neither GST-NPY nor GST-NPY hexamers are expected to behave exactly as the 36 amino acid circulating NPY, but adequate visualization of unlabeled NPY is not possible using LC-TEM at this stage. GST-NPY assemblies retain the capacity to bind N3 and N2 and were thus used as a proxy for NPY which could more easily be imaged. Also, due to their size and multivalency, GST-NPY hexamers enable more facile visualization of motion in NPY tethers, especially rotational motion, which would otherwise be imperceptible from translational motion in a singly valent analyte.

In some experiments, GST-NPY assemblies were labeled with N2−Au (using procedure discussed before) to increase contrast and enhance both bright-field and dark-field images. Motion of GST-NPY assemblies captured near the graphene surface by BREs are imaged in bright-field mode, as shown in Figure 3 and Supporting Information Video V1. For these experiments, electron dose was kept below damage thresholds for the protein. A detailed discussion of beam damage and dose effects is included in the Supporting Information Section 3.3.

To visualize NPY as captured by BREs on working devices, BRE was first coupled to graphene via PBASE. NPY was coupled to BRE on the TEM chip with GST-NPY solutions in water. To facilitate imaging, GST-NPY was then labeled with N2−Au in water. The positions of the GST-NPY assemblies were tracked over time as shown in Figure 3. Figure 3A shows a series of images containing four representative graphene-bound assemblies. Figure 3B shows a plot of the positions of the NPY centroids relative to the average centroid position over time. Figure 3C plots the step distances observed between successive frames. The assembly tracking analysis reveals heterogeneous motion in captured assemblies. In the field of view shown, two assemblies (C,D) are relatively stationary over the course of the 74 s video, whereas assemblies A,B show more dynamic motion. Assembly A showed a range of motion within an approximately 5.5 nm radius, whereas assembly B exhibited a larger range of motion with positions up to 10 nm away from the average centroid position.

These observations fall within the maximum expected tether length based on the BREs of the system. Specifically, there are three potential tether lengths. PBASE conjugation to P1N3 at the N terminus produces a tether that is 27 amino acids in length. PBASE conjugation to P1N3 at Lys11 produces a tether length of 16 amino acids. The third tether length results from P1N3 direct coupling to the graphene surface. Assuming full interaction of the P1 domain of P1N3 with the graphene surface, a tether length of 15 amino acids is expected. The assembly tracking analyses in Figure 3 suggest two distinct tether lengths of approximately 5.5 and 10 nm. These observed lengths reasonably match expected tether lengths resulting from peptide chains of 16 and 27 amino acids assuming an extended peptide conformation with an inter-residue spacing of 3.5 Å (5.6 and 9.45 nm, respectively).[39] Tether lengths corresponding to 15 and 16 amino acids, even if both are present in these samples, are likely similar enough in length that they may not be distinguishable by these methods. A much larger sampling of assembly trajectories would need to be analyzed to substantiate the claim that tether length of captured analytes can be directly measured but tether lengths of other molecules (DNA) have been estimated before using fluorescence imaging and similar analysis.[40] In any case, the direct observation of a number of distinct tethering behaviors suggests that direct imaging could play a role in understanding biosensor performance.

LC-TEM observations were also made of NPY assemblies captured by BREs directly coupled to graphene via the P1 domain of P1N3, omitting PBASE as BRE-graphene linker. Labeling with gold was also omitted so that the system more closely matched real-world devices. Assemblies coupled directly to graphene via P1N3 appeared confined to similar positional envelopes as those coupled using PBASE as linker. Assemblies were generally confined in both cases to envelopes with radii of approximately 5 and 10 nm. These limited observations suggest the likelihood of only minor differences in sensor performance due to these two distinct coupling strategies (see Figures 5 and S10). In addition to tracking positional envelopes, qualitative data was also collected on the motion of captured analyte (see Supporting Information, Videos 1 and 4). Direct visualization revealed apparently stochastic positional fluctuations of assemblies within a circular envelope as well as assembly rotations. These observations provide information which is potentially valuable toward understanding the sources of noise or transients in the sensor response in a number of analyte capture strategies. Recent theoretical studies consider association and dissociation of the analytes as the only source of noise,[41−44] however the role of rotational motion of captured analyte on sensor surfaces or of variability in radius of the positional fluctuation envelope on sensor noise is yet to be investigated in detail. Similar to association and dissociation of analyte, motion in a direction perpendicular to the sensor surface is expected to add noise as the analyte goes in and out of the Debye length.[43,44] LC-TEM, especially on functional GFET devices, appears poised to enable these investigations.

***In Operando* LC-TEM Study.** Figure 4 presents the results of probing graphene's conductivity while simultaneously visualizing changes in surface decoration of the graphene via LC-TEM. TEM chips were coated with graphene and then directly functionalized with P1N3 for NPY capture. Prior to electrical measurements, devices were incubated with GST-NPY and N2-Au. Perfusion rates of 0.5 and 2 μL/min resulted

DOI: 10.1021/acsami.8b20498
ACS Appl. Mater. Interfaces 2019, 11, 13927−13934

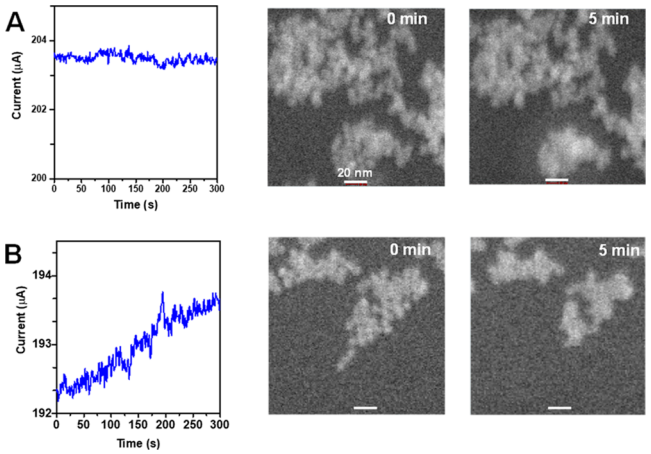

Figure 4. Simultaneous LC-TEM and potentiometry of NPY captured onto and released from GFET surface. Panel A shows the effect of low flow perfusion of BRE-functionalized graphene devices with captured, gold-tagged analyte. Over a 5 min experiment, little to no change in surface decoration is observed with corresponding constant current through the GFET device with 0.2 V V_{SD} and 0 V V_{GS}. In contrast, panel B shows the effect of faster perfusion which disrupts the BRE-analyte-tag assemblies on the graphene surface, resulting in increases in current through the device. See Supporting Information Videos V2 and V3 for temporal evolution of assemblies. All scale bars are 20 nm.

in differences in BRE-analyte-tag retention on the surface, with the higher perfusion rate disrupting and washing away the Au nanoparticles and likely the complete NPY-Au complexes from the surface. Accumulation of analyte on the surface with concurrent electrical measurement is not shown due to the longer accumulation times required to capture the analyte and the more extensive beam damage resulting from longer accumulation times. Nevertheless, a correlation between conductivity and surface decoration in P1N3-GFET devices is evident.

Selectivity and Sensitivity Study. The response of GFET devices in the LC-TEM chips to NPY is examined in detail here using GFET devices made on silicon substrates (see Section S2.3 for details on sample preparation). The response to NPY was also compared with IL-6, which is another relevant biomarker but potential interferent to specific NPY detection. IL-6, a 20.9 kDa protein with high alpha helical content, has been measured in human sweat in ranges of 10−100 pg/mL,[24] corresponding to approximately 0.5−5 pM. An electrolyte-gating scheme, as shown in the inset in Figure 5A, was employed with static artificial perspiration as electrolyte (AP, Pickering laboratories, CA, U.S.A.). Current through the graphene layer was measured while the gate potential was swept from +ve to −ve with an applied source/drain (S/D) bias of 0.3 V. As an additional control, GFET devices functionalized with only the graphene binding domain P1 were exposed to NPY. As seen in Figure 5A, NPY additions to P1N3-GFET devices in the picomolar range shifted both graphene's Dirac voltage (V_{Dirac}) and conductivity over a wide range of gate voltages. These shifts remained similar even when PBASE was used as a linker between graphene and P1N3 or when NPY-GST assembly was used as analyte (see Supporting

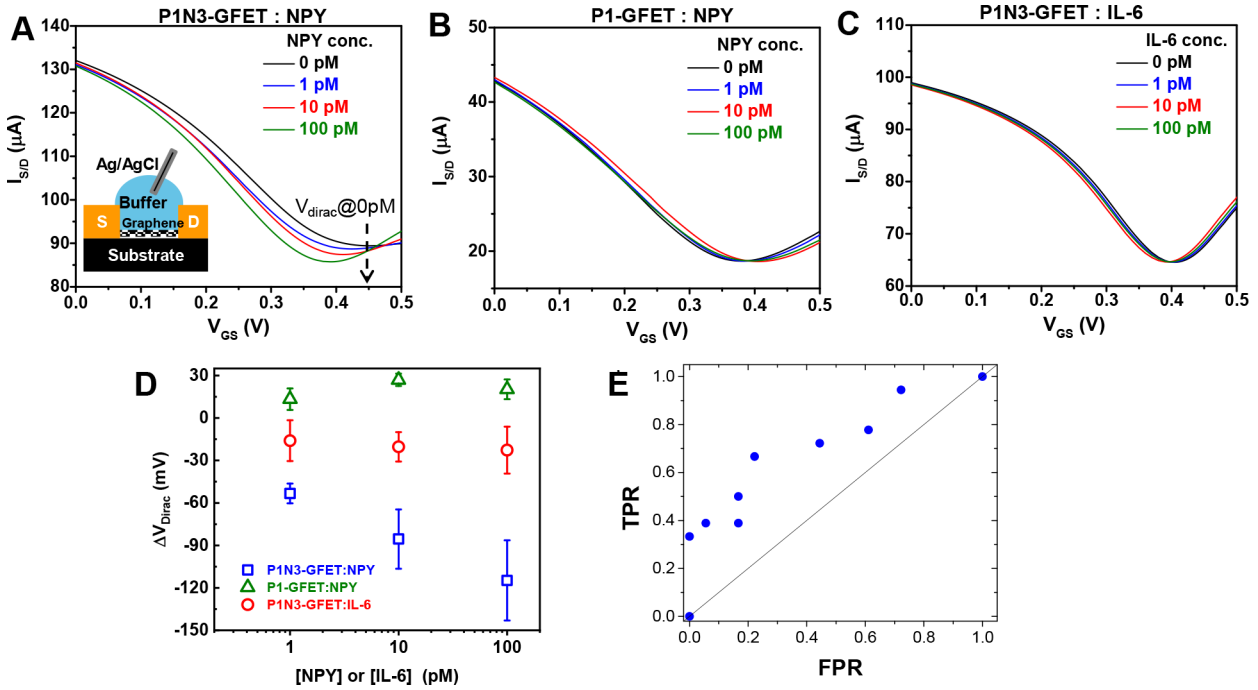

Figure 5. GFET responses to BRE-NPY binding. Panel A plots the source/drain (S/D) current versus gate/source (G/S) voltage in a GFET functionalized with the bidomain peptide P1N3 with affinity to both graphene and neuropeptide Y. Both a change in the charge neutrality point of graphene (i.e. Dirac voltage,V_{Dirac}) and changes in graphene's conductivity were observed upon NPY administration. V_{Dirac} at 0 pM NPY is indicated with an arrow. Inset illustrates device setup with electrolyte-gating. Panels B and C show negative control devices with non-NPY binding P1 (B) and P1N3 in response to IL-6 (C). In both cases, V_{Dirac} changes are insignificant compared to changes observed in (A). Panel D shows the result of plotting V_{Dirac} versus the analyte concentrations for the data shown in (A) through (C). The response of the NPY-selective GFET based on P1N3 is markedly steeper than the responses of either negative control. Panel E shows a receiver operator characteristic (plotting true positive rate TPR versus false positive rate FPR of the response curve) for a P1N3-GFET device exposed to 18 positive and 18 negative samples, demonstrating its utility for NPY biosensing.

DOI: 10.1021/acsami.8b20498
ACS Appl. Mater. Interfaces 2019, 11, 13927−13934

Information, Figures S10–S11). On the other hand, addition of NPY to P1-GFET devices (Figure 5B) and addition of IL-6 to P1N3-GFET devices (Figure 5C) show negligible changes in V_{Dirac} and conductivity. Any shifts in the $I-V$ curves for these negative controls did not appear to be dose responsive.

Changes in V_{Dirac} are plotted as a function of NPY (or IL-6) concentration in Figure 5D, which suggests the utility of P1N3-GFET as a sensitive device for NPY biosensing. In only the case of the P1N3-GFET response, consistent sensitivity to NPY can be observed over the tested range. In contrast, the response to the P1N3-GFET to IL-6 is flat. These two experiments suggest that P1N3-GFET devices can be both sensitive and selective to NPY in sweat, although more selectivity studies are needed to fully qualify P1N3-GFETs for real-world use. The response of P1-GFET to NPY is also encouraging in that there is no significant response without the NPY-specific BRE. In this case, only a slight change in Dirac voltage is observed over the tested range, yet the change does not appear to trend with analyte concentration. This result suggests that the NPY in P1N3-GFET experiments is likely interacting with the N3 domain and that the P1N3-GFET response is not likely due to nonspecific adsorption of NPY to the graphene surface or to the P1 domain. Instead, changes in Dirac voltage of P1-GFETs to NPY likely hint at other nonspecific interactions with graphene that require further elucidation; for example, charge screening effects of varied salt concentrations or charged amino acids in solution may alter graphene conductivity and Dirac voltage without adsorption to the graphene surface or its capture peptides. Further experiments, potentially using LC-TEM, are required to elucidate these effects and to devise effective counter-measures.

Continuous Monitoring of NPY. Static measurements simulate conditions pertinent to scenarios with accumulated analyte or for spot assessments, such as for single use sweat patches. For continuous monitoring applications, continuous flow experimental apparatus such as in Figure 5E are more appropriate. To this end, a microfluidic delivery apparatus was employed to perfuse the P1N3-GFET with NPY-spiked AP. Eighteen positive samples, defined as containing 10 pM NPY and higher, and 18 negative samples comprised of 1 pM NPY or 10–100 pM IL-6 were tested and used to generate a receiver operator characteristic (ROC) curve. Former analytes were washed away prior to testing each new sample by flowing Tris-buffered saline (TBS) for 30 min through the microfluidic chamber and then heating to 55 °C. The chip was then equilibrated again in TBS buffer under constant flow for at least 45 min. (See Section S4.2 for complete details.) The positive/negative distinction threshold was derived from the maximum rate of change in the step response of the sensor from negative AP solution to the test sample. Sweeping through a range of cutoff maximum rates of change and then classifying each sample as greater or less than 10 pM, in comparison to the known concentrations enables the plotting of the true positive rate (TPR) versus false positive rate (FPR) for the collective data set. The area under the curve indicates the fitness of a given sensor for use. Classifying NPY or IL-6 samples using a cutoff threshold of 10 pM resulted in an area under the ROC curve of 0.74. This is similar to the results obtained from graphene FETs (see Section S4.3) and other diagnostic devices functionalized with antibodies; short peptide BREs used in this study however have the benefit of potentially longer shelf life and lower cost of production.[11]

CONCLUSIONS

The data presented in this paper allows a number of useful conclusions. First, we observed that functionalization of graphene FET devices for specific capture of NPY can be done directly with bidomain peptides. We presented a specific BRE, P1N3, which can be used to functionalize GFET devices to produce a biosensor device with pM sensitivity to the neuropeptide NPY. Notably, biosensors based on N3 coupled to quartz crystal microbalance only showed micromolar responsivity to NPY in our hands (see Supporting Information, Section S1.2). In addition, selectivity of P1N3 GFETs for NPY has been shown against the background of a small set of control experiments, although more specificity validation would be required to establish P1N3-GFET for NPY sensing in sweat.

We further showed that LC-TEM enables the direct observation of assembly motion and abundance. This will allow for the collection of statistically valid analyses of the fraction of captured molecules which are tightly bound to the surface versus the number of molecules with confined Brownian motion, potentially including the actual tether lengths if enough molecules are tracked. We observed that assembly motion between two different tether strategies was qualitatively similar and we noted a likelihood that the two sensor systems would perform similarly, which was borne out experimentally. Additionally, none of the observed envelopes exceeded the expected molecular tether length, suggesting that the motion we observe is due to constrained Brownian motion and that measurement of motion on a large number of assemblies might enable the estimation of tether length. The observations presented in this work are potentially meaningful as proof of concept toward novel approaches to understanding the mechanisms that impact biosensor performance. Finally, these approaches are likely applicable to other technology areas including enzyme encapsulation, catalysis, antifouling surfaces, clinical assays, and functional substrates.

ASSOCIATED CONTENT

Supporting Information

The Supporting Information is available free of charge on the ACS Publications website at DOI: 10.1021/acsami.8b20498.

Detailed descriptions of isolation and characterization of peptides, graphene processing, imaging conditions, electrical measurements, used chemicals and reagents (PDF)

Video of protein assembly trajectory (AVI)

Video of protein assembly trajectory (AVI)

Video of retention and release of proteins from graphene surfaces (AVI)

Video of retention and release of proteins from graphene surfaces (AVI)

AUTHOR INFORMATION

Corresponding Author

*E-mail: lawrence.drummy.1@us.af.mil.

ORCID

Steve Kim: 0000-0002-9519-077X

Ming-Siao Hsiao: 0000-0001-9319-653X

Nancy Kelley-Loughnane: 0000-0003-2974-644X

Rajesh R. Naik: 0000-0002-7677-928X

Lawrence F. Drummy: 0000-0002-6452-5768

DOI: 10.1021/acsami.8b20498
ACS Appl. Mater. Interfaces 2019, 11, 13927–13934

Present Address

[¶](M.-S.H.) DuPont, Circleville, OH 43113.

Author Contributions

[#]S.K. and L.X. contributed equally.

Funding

The authors acknowledge the Air Force Research Laboratory for funding.

Notes

The authors declare no competing financial interest.

REFERENCES

(1) Zhou, L.; Mao, H.; Wu, C.; Tang, L.; Wu, Z.; Sun, H.; Zhang, H.; Zhou, H.; Jia, C.; Jin, Q.; Chen, X.; Zhao, J. Label-Free Graphene Biosensor Targeting Cancer Molecules Based on Non-Covalent Modification. *Biosens. Bioelectron.* **2017**, *87*, 701−707.

(2) Khatayevich, D.; Page, T.; Gresswell, C.; Hayamizu, Y.; Grady, W.; Sarikaya, M. Selective Detection of Target Proteins by Peptide-Enabled Graphene Biosensor. *Small* **2014**, *10* (8), 1505−1513.

(3) Cui, Y.; Kim, S. N.; Naik, R. R.; McAlpine, M. C. Biomimetic Peptide Nanosensors. *Acc. Chem. Res.* **2012**, *45* (5), 696−704.

(4) Fu, W.; Jiang, L.; van Geest, E. P.; Lima, L. M.; Schneider, G. F. Sensing at the Surface of Graphene Field-Effect Transistors. *Adv. Mater.* **2017**, *29* (6), 1603610.

(5) Kim, J. E.; No, Y. H.; Kim, J. N.; Shin, Y. S.; Kang, W. T.; Kim, Y. R.; Kim, K. N.; Kim, Y. H.; Yu, W. J. Highly Sensitive Graphene Biosensor by Monomolecular Self-Assembly of Receptors on Graphene Surface. *Appl. Phys. Lett.* **2017**, *110* (20), 203702.

(6) Lei, Y. M.; Xiao, M. M.; Li, Y. T.; Xu, L.; Zhang, H.; Zhang, Z. Y.; Zhang, G. J. Detection of Heart Failure-Related Biomarker in Whole Blood with Graphene Field Effect Transistor Biosensor. *Biosens. Bioelectron.* **2017**, *91*, 1−7.

(7) de Jonge, N.; Peckys, D. B.; Kremers, G. J.; Piston, D. W. Electron Microscopy of Whole Cells in Liquid with Nanometer Resolution. *Proc. Natl. Acad. Sci. U. S. A.* **2009**, *106* (7), 2159−2164.

(8) Proetto, M. T.; Rush, A. M.; Chien, M. P.; Abellan, B. P.; Patterson, J. P.; Thompson, M. P.; Olson, N. H.; Moore, C. E.; Rheingold, A. L.; Andolina, C.; Millstone, J.; Howell, S. B.; Browning, N. D.; Evans, J. E.; Gianneschi, N. C. Dynamics of Soft Nanomaterials Captured by Transmission Electron Microscopy in Liquid Water. *J. Am. Chem. Soc.* **2014**, *136* (4), 1162−1165.

(9) Cameron Varano, A.; Rahimi, A.; Dukes, M. J.; Poelzing, S.; S, M. M.; Kelly, D. F. Visualizing Virus Particle Mobility in Liquid at the Nanoscale. *Chem. Commun. (Cambridge, U. K.)* **2015**, *51* (90), 16176−16179.

(10) Ross, F. M. Opportunities and Challenges in Liquid Cell Electron Microscopy. *Science* **2015**, *350* (6267), No. aaa9886.

(11) Ladner, R. C.; Sato, A. K.; Gorzelany, J.; de Souza, M. Phage Display-derived Peptides as Therapeutic Alternatives to Antibodies. *Drug Discovery Today* **2004**, *9* (12), 525−529.

(12) Pande, J.; Szewczyk, M. M.; Grover, A. K. Phage Display: Concept, Innovations, Applications and Future. *Biotechnol. Adv.* **2010**, *28* (6), 849−858.

(13) Dudak, F. C.; Boyaci, I. H.; Orner, B. P. The Discovery of Small-Molecule Mimicking Peptides Through Phage Display. *Molecules* **2011**, *16* (1), 774−789.

(14) Schirrmann, T.; Meyer, T.; Schutte, M.; Frenzel, A.; Hust, M. Phage Display for the Generation of Antibodies for Proteome Research, Diagnostics and Therapy. *Molecules* **2011**, *16* (1), 412−426.

(15) Deutscher, S. L. Phage display in molecular imaging and diagnosis of cancer. *Chem. Rev.* **2010**, *110* (5), 3196−211.

(16) Li, W.; Caberoy, N. B. New Perspective for Phage Display As an Efficient and Versatile Technology of Functional Proteomics. *Appl. Microbiol. Biotechnol.* **2010**, *85* (4), 909−919.

(17) Cui, Y.; Kim, S. N.; Jones, S. E.; Wissler, L. L.; Naik, R. R.; McAlpine, M. C. Chemical Functionalization of Graphene Enabled by Phage Displayed Peptides. *Nano Lett.* **2010**, *10* (11), 4559−4565.

(18) Jaworski, J. W.; Raorane, D.; Huh, J. H.; Majumdar, A.; Lee, S. W. Evolutionary screening of biomimetic coatings for selective detection of explosives. *Langmuir* **2008**, *24* (9), 4938−4943.

(19) Naik, R. R.; Stringer, S. J.; Agarwal, G.; Jones, S. E.; Stone, M. O. Biomimetic synthesis and patterning of silver nanoparticles. *Nat. Mater.* **2002**, *1* (3), 169−172.

(20) Sarikaya, M.; Tamerler, C.; Jen, A. K. Y.; Schulten, K.; Baneyx, F. Molecular biomimetics: nanotechnology through biology. *Nat. Mater.* **2003**, *2* (9), 577−585.

(21) Sajdyk, T. J.; Shekhar, A.; Gehlert, D. R. Interactions between NPY and CRF in the Amygdala to Regulate Emotionality. *Neuropeptides* **2004**, *38* (4), 225−234.

(22) Reichmann, F.; Holzer, P. Neuropeptide Y: A stressful review. *Neuropeptides* **2016**, *55*, 99−109.

(23) Sabban, E. L.; Alaluf, L. G.; Serova, L. I. Potential of neuropeptide Y for preventing or treating post-traumatic stress disorder. *Neuropeptides* **2016**, *56*, 19−24.

(24) Cizza, G.; Marques, A. H.; Eskandari, F.; Christie, I. C.; Torvik, S.; Silverman, M. N.; Phillips, T. M.; Sternberg, E. M.; Group, P. S. Elevated Neuroimmune Biomarkers in Sweat Patches and Plasma of Premenopausal Women with Major Depressive Disorder in Remission: The Power Study. *Biol. Psychiatry* **2008**, *64* (10), 907−911.

(25) Xu, G. Y.; Abbott, J.; Qin, L.; Yeung, K. Y. M.; Song, Y.; Yoon, H.; Kong, J.; Ham, D. Electrophoretic and field-effect graphene for all-electrical DNA array technology. *Nat. Commun.* **2014**, *5*, 5.

(26) Gao, Z. L.; Xia, H.; Zauberman, J.; Tomaiuolo, M.; Ping, J. L.; Zhang, Q. C.; Ducos, P.; Ye, H. C.; Wang, S.; Yang, X. P.; Lubna, F.; Luo, Z. T.; Ren, L.; Johnson, A. T. C. Detection of Sub-fM DNA with Target Recycling and Self-Assembly Amplification on Graphene Field-Effect Biosensors. *Nano Lett.* **2018**, *18* (6), 3509−3515.

(27) Vodnik, M.; Zager, U.; Strukelj, B.; Lunder, M. Phage display: selecting straws instead of a needle from a haystack. *Molecules* **2011**, *16* (1), 790−817.

(28) Funke, S. A.; Willbold, D. Mirror Image Phage Display–A Method to Generate D-Peptide Ligands for Use in Diagnostic or Therapeutical Applications. *Mol. BioSyst.* **2009**, *5* (8), 783−786.

(29) Pender, M. J.; Sowards, L. A.; Hartgerink, J. D.; Stone, M. O.; Naik, R. R. Peptide-Mediated Formation of Single-Wall Carbon Nanotube Composites. *Nano Lett.* **2006**, *6* (1), 40−44.

(30) Talavera, D.; Robertson, D. L.; Lovell, S. C. Characterization of protein-protein interaction interfaces from a single species. *PLoS One* **2011**, *6* (6), No. e21053.

(31) Devlin, J. J.; Panganiban, L. C.; Devlin, P. E. Random Peptide Libraries: A Source of Specific Protein Binding Molecules. *Science* **1990**, *249* (4967), 404−406.

(32) Mirau, P. A.; Naik, R. R.; Gehring, P. Structure of Peptides on Metal Oxide Surfaces Probed by NMR. *J. Am. Chem. Soc.* **2011**, *133* (45), 18243−18248.

(33) Islam, A. E.; Kim, S. S.; Rao, R.; Ngo, Y.; Jiang, J.; Nikolaev, P.; Naik, R.; Pachter, R.; Boeckl, J.; Maruyama, B. Photo-thermal Oxidation of Single Layer Graphene. *RSC Adv.* **2016**, *6* (48), 42545−42553.

(34) Kim, S. S.; Kuang, Z.; Ngo, Y. H.; Farmer, B. L.; Naik, R. R. Biotic-Abiotic Interactions: Factors that Influence Peptide-Graphene Interactions. *ACS Appl. Mater. Interfaces* **2015**, *7* (36), 20447−20453.

(35) Chen, R. J.; Zhang, Y.; Wang, D.; Dai, H. Noncovalent Sidewall Functionalization of Single-Walled Carbon Nanotubes for Protein Immobilization. *J. Am. Chem. Soc.* **2001**, *123*, 3838−3839.

(36) Katz, E. Application of bifunctional reagents for immobilization of proteins on a carbon electrode surface - oriented immobilization of photosynthetic reaction centers. *J. Electroanal. Chem.* **1994**, *365* (1−2), 157−164.

(37) Gao, Z. L.; Kang, H.; Naylor, C. H.; Streller, F.; Ducos, P.; Serrano, M. D.; Ping, J. L.; Zauberman, J.; Rajesh, Carpick R. W.; Wang, Y. J.; Park, Y. W.; Luo, Z. T.; Ren, L.; Johnson, A. T. C.; et al. Scalable Production of Sensor Arrays Based on High-Mobility Hybrid Graphene Field Effect Transistors. *ACS Appl. Mater. Interfaces* **2016**, *8* (41), 27546−27552.

DOI: 10.1021/acsami.8b20498
ACS Appl. Mater. Interfaces 2019, 11, 13927−13934

(38) Sengupta, J.; Bussiere, C.; Pallesen, J.; West, M.; Johnson, A. W.; Frank, J. Characterization of The Nuclear Export Adaptor Protein Nmd3 in Association with The 60s Ribosomal Subunit. *J. Cell Biol.* **2010**, *189* (7), 1079−1086.
(39) Pauling, L.; Corey, R. B.; Branson, H. R. The Structure of Proteins: Two Hydrogen-Bonded Helical Configurations of the Polypeptide Chain. *Proc. Natl. Acad. Sci. U. S. A.* **1951**, *37* (4), 205−211.
(40) Pouget, N.; Dennis, C.; Turlan, C.; Grigoriev, M.; Chandler, M.; Salome, L. Single-particle tracking for DNA tether length monitoring. *Nucleic Acids Res.* **2004**, *32* (9), No. e73.
(41) Hassibi, A.; Zahedi, S.; Navid, R.; Dutton, R. W.; Lee, T. H. Biological shot-noise and quantum-limited signal-to-noise ratio in affinity-based biosensors. *J. Appl. Phys.* **2005**, *97* (8), 084701.
(42) Hassibi, A.; Vikalo, H.; Hajimiri, A. On noise processes and limits of performance in biosensors. *J. Appl. Phys.* **2007**, *102* (1), 014909.
(43) Zhang, D.; Solomon, P.; Zhang, S. L.; Zhang, Z. Correlation of Low-Frequency Noise to the Dynamic Properties of the Sensing Surface in Electrolytes. *Acs Sensors.* **2017**, *2* (8), 1160−1166.
(44) Tulzer, G.; Heitzinger, C. Fluctuations due to association and dissociation processes at nanowire-biosensor surfaces and their optimal design. *Nanotechnology* **2015**, *26* (2), 025502.

DOI: 10.1021/acsami.8b20498
ACS Appl. Mater. Interfaces 2019, 11, 13927−13934